The influence of lateral transport on sedimentary alkenone paleoproxy signals

Blanca Ausín[1,2], Negar Haghipour[2,3], Elena ~~Bruni~~[1]Bruni[2], Timothy Eglinton[1,2]

[1]Geology Department, Salamanca University, Salamanca, 37008, Spain

[2]Earth Sciences Department, ETH Zurich, Zurich, 8092, Switzerland

[3]Laboratory of Ion Beam Physics, ETH Zurich, Zurich, 8092, Switzerland

Correspondence to: Blanca Ausín (ausin@usal.es)

Abstract. Alkenone signatures preserved in marine sedimentary records are considered one of the most robust paleothermometers ~~available, and~~available and are often used as a proxy for paleoproductivity. However, important gaps remain regarding~~on~~ the provenance and fate of alkenones, and their impact on derived environmental signals in marine sediments. Here, we analyze the abundance, distribution, and radiocarbon (^{14}C) age of alkenones in bulk sediments and corresponding grain-size fractions in surficial sediments from seven continental margin settings in the Pacific and Atlantic Oceans ~~in order to~~to evaluate the impact of organo-mineral associations and hydrodynamic sorting on sedimentary alkenone signals. We find that alkenones preferentially reside within fine-grained mineral fractions of continental margin sediments, with the preponderance of alkenones residing within the fine silt fraction (2-10 μm), and most strongly influencing alkenone ^{14}C age, and SST signals from bulk sediments as a consequence of their proportional abundance and higher degree of organic matter (OM) protection relative to other fractions. Our results ~~demonstrate~~ provide further evidence ~~that~~ for the key role of selective association of alkenones with mineral surfaces and associated hydrodynamic mineral sorting processes ~~can alter~~on the reliability of alkenone signals encoded in marine sediments (^{14}C age, content, and distribution) and ~~confound~~ the fidelity of corresponding proxy records (productivity and sea surface temperature (SST)) in the spatial and temporal domain.

1. Introduction

Since the initial discovery of alkenones [*Boon et al.*, 1978; *Volkman et al.*, 1980], these molecular biomarkers have become one of the most applied and well-established paleoclimate proxies, allowing estimation of sea surface temperature (SST) and primary productivity in most oceanographic settings [*Raja and Rosell-Melé*, 2021; *Sachs et al.*, 2000]. Alkenones are long chain (C_{37}-C_{39}) unsaturated ketones synthesized by some species of haptophytes dwelling in the upper photic zone, most notably the coccolithophore species *Emiliania huxleyi* and *Gephyrocapsa oceanica* [*Volkman et al.*, 1980].

The total abundance of C_{37} alkenones ($C_{37:2}$ + $C_{37:23}$) in marine sediments is widely used as a qualitative proxy for primary productivity on the basis that alkenones are a large component of the total carbon of *Emiliania huxleyi* [*Fredrick G. Prahl et*

al., 1988], and that alkenone degradation is not observed upon zooplankton digestion [*Grice et al.*, 1998; *Grimalt et al.*, 2000; *Volkman et al.*, 1980]. However, this signal can be altered in marine sediments by the significant loss of alkenones that occurs during their export to and deposition on the seafloor. This "flux attenuation" is site-dependent and generally higher during periods of maximum flux [*Rosell-Melé and Prahl*, 2013]. An additional process that may influence this paleoproductivity indicator includes alkenone input via lateral transport of suspended particles and sediments, which has proven to significantly bias the temperature signal on the Argentine continental margin [*Benthien and Müller*, 2000] and the Bermuda Rise [*Nao Ohkouchi et al.*, 2002]. Since the latter work, the influence of lateral transport on the radiocarbon (^{14}C) age of sedimentary alkenones was increasingly assessed in other oceanic settings, revealing ^{14}C age offsets among alkenones and other co-occurring proxy-bearing marine particles due to their secondary transport is a widespread phenomenon in bottom sediments of the world's oceans [e.g., *Kusch et al.*, 2010; *Gesine Mollenhauer et al.*, 2007; *Gesine Mollenhauer et al.*, 2005]. However, a specific determination of the sediment size fraction in which alkenones may preferentially reside is lacking [*Sachs et al.*, 2000]. Given the propensity for preferential mobilization and ~~redistribution~~redistribution of specific grain sizes [*Bao et al.*, 2016; *McCave and Hall*, 2006a; *McCave et al.*, 1995; *Pedrosa-Pàmies et al.*, 2013] this information is crucial for assessing potential impacts on sedimentary alkenone signals.

The degree of unsaturation of the C_{37} alkenones, parameterized through the $U^{k'}_{37}$ ratio (Eq. 1), varies as a function of the growth temperature of the precursor organisms.

$$Uk'37 = \frac{[C37{:}2]}{[C37{:}2]+[C37{:}3]} \quad \text{Eq. (1)}$$

where $[C_{37:2}]$ and $[C_{37:3}]$ are the concentrations of di- and tri-unsaturated C_{37} alkenones, respectively.

The relationship between $U^{k'}_{37}$ and SST was first quantified in laboratory cultures [*F. G. Prahl and Wakeham*, 1987] with a reported precision of ±0.5~~6~~°C, leading to the implementation of global calibrations of the $U^{k'}_{37}$ ratio from marine surface sediments with instrumental SSTs [*Conte et al.*, 2006; *Müller et al.*, 1998; *Tierney and Tingley*, 2018]. The latter calibration curves exhibit larger associated errors because core-top SST does not always effectively record annual average SST from the overlying water column. In regions like the North Atlantic (>48°N), North Pacific (>45°N), Mediterranean Sea, and the Black Sea, systematic $U^{k'}_{37}$-SST decoupling with surface water temperature has been attributed to factors such as seasonal biases in haptophyte productivity and dissolved nutrient concentrations [*Epstein et al.*, 1998], highlighting the need for seasonally-tuned calibrations [*Tierney and Tingley*, 2018]. Selective degradation of the $C_{37:3}$ due to free radical oxidation and aerobic bacterial processes [*Rontani et al.*, 2013; *Zabeti et al.*, 2010] may result in ~~warmer bias~~warm biases in some settings such as SE Alaska, the eastern Pacific, and Santa Monica Basin [*Gong and Hollander*, 1999; *Jaeschke et al.*, 2017; *F. G. Prahl et al.*, 2010]. In other regions, such as the Brazil-Malvinas confluence [*Benthien and Müller*, 2000; *Rühlemann and Butzin*, 2006], the Nordic and Labrador Seas [*Bendle and Rosell-Melé*, 2004; *Filippova et al.*, 2016; *Tierney and Tingley*, 2018] and northern Sargasso Sea [*Nao Ohkouchi et al.*, 2002]~~[*Ohkouchi et al., 2002*],~~ marked SST deviations have been attributed to lateral advection of alkenones synthesized in distal regions characterized by distinct surface ocean temperatures. In this regard, the implementation of a general ocean circulation model indicated that long particle residence times and lateral advection of alkenones (via OM-

mineral interaction) could strongly decouple sediment $U^{k'}_{37}$-SST and overlying surface water temperature on continental shelves [*Rühlemann and Butzin*, 2006]. Similarly, advection of pre-aged alkenones associated with mineral surfaces is typically invoked to explain older radiocarbon ages of alkenones in relation to coeval foraminifera in many continental margin and deep ocean settings [e.g., *Ausín et al.*, 2019; *Kusch et al.*, 2010; *G. Mollenhauer et al.*, 2003; *Gesine Mollenhauer et al.*, 2005].

Sediments deposited on continental margins are the focus of numerous paleoceanographic studies due to the expanded temporal resolution that they offer over deep-sea sedimentary sequences, they thus dominate global calibration data. Yet, an in-depth investigation of the coupled effects of alkenone-mineral associations and hydrodynamic processes (e.g., resuspension and lateral transport) on alkenone-based proxy signals recorded in continental margin sediments has not yet been undertaken. Recent studies have highlighted how the interplay between organo-mineral relationships and the grain-size dependent hydrodynamic mineral particle sorting effects exerts strong control on the content and geochemical signatures of OC (organic carbon) in continental margin surface sediments [*Ausín et al.*, 2021; *Bao et al.*, 2018b; *Bröder et al.*, 2018; *Magill et al.*, 2018]. In general, fine-grained minerals host higher amounts of OM than larger particles by virtue of their higher surface area and hence enhanced physical protection against OM remineralization [*Hedges and Keil*, 1995; *R.G. Keil and Mayer*, 2014; *Richard G. Keil et al.*, 1994b; *Mayer*, 1994a; b]. Additionally, the size of mineral particles and their propensity for resuspension largely determines their tendency to be remobilized and dispersed at a given bed shear stress [*McCave and Hall*, 2006a]. Consequently, hydrodynamic particle sorting processes not only selectively translocate OC sorbed to minerals but also expose it to further degradation [*Ausín et al.*, 2021; *Bao et al.*, 2016; *Bao et al.*, 2018a; *Bao et al.*, 2018b]. As a component of this OC, alkenones associated with specific grain-size fractions are subject to dispersal and decomposition as a function of the governing hydrodynamic conditions that delineate sediment transport pathways and deposition patterns. Given that the strength and trajectory of mobilizing currents may vary as a function of ocean and climate conditions, and considering continental margins are strategic locations for high-temporal-resolution paleoceanographic investigations, greater understanding of the influence of these mechanisms on alkenone signals encoded in marine sediments is needed to improve interpretations of derived proxy records. Here, we explore alkenone-mineral grain-size relationships in a suite of surficial sediment samples from seven locations, mostly on productive continental margins, where geochemical evidence exists for the influence of organo-mineral relationships and hydrodynamic particle sorting on OC geochemical signatures and content [*Ausín et al.*, 2021].

2. Materials and Methods

2.1. Surface sediment samples

Six surface and one near-surface sediment samples were obtained from five different continental margin settings and one deep-ocean sediment drift (Fig. 1; Table 1). A detailed description of the depositional setting and environmental characteristics of each study site can be found in Ausín et al. [2021]. The Peruvian margin site ("PER") is characterized by persistent upwelling that supports very high primary productivity and sustains low oxygen bottom waters [*Reimers and Suess*, 1983]. Sites from

Santa Barbara and Santa Monica Basins ("SBB" and "SMB") in the highly productive California margin also feature sub-oxic to anoxic bottom waters favoring OM preservation in underlying sediments. The site abbreviated as "NAT" is from the New England "Mud Patch", a shelf depocenter south of Cape Cod on the Mid-Atlantic Bight that is characterized by moderately high surface ocean productivity and rapid fine-grained deposition under oxic conditions [*Goff et al.*, 2019; *Twichell et al.*, 1981]. The Namibian margin is characterized by strong upwelling and high primary productivity, and the study site "NAM" is under sporadic influence of high-productivity filaments from the adjacent Lüderitz upwelling cell and is located in an OC depocenter on the upper slope produced by the offshore transport of shelf sediments [*Inthorn et al.*, 2006a]. The deep-ocean site "BER" from the Bermuda Rise in the sub-tropical NW Atlantic is characterized by low primary productivity in overlying surface waters and a ~~a~~ fully oxygenated water column~~-~~. This contourite deposit stems from currents associated with deep-ocean recirculation gyres that result in focused deposition of fine-grained sediment [*Laine and Hollister*, 1981; *Laine et al.*, 1994]. The site named as "NAF", on the NW African margin, is influenced by the Canary Current Upwelling system featuring moderate productivity and bottom water oxygen contents [*Zonneveld et al.*, 2010]. Advective sediment transport has been proposed to explain the relatively low settling rates of coccolithophore calcite plates and alkenones [*Fischer et al.*, 2009], in contrast ~~with~~ to the minor or negligible presence of pre-aged alkenones [*Gesine Mollenhauer et al.*, 2005].

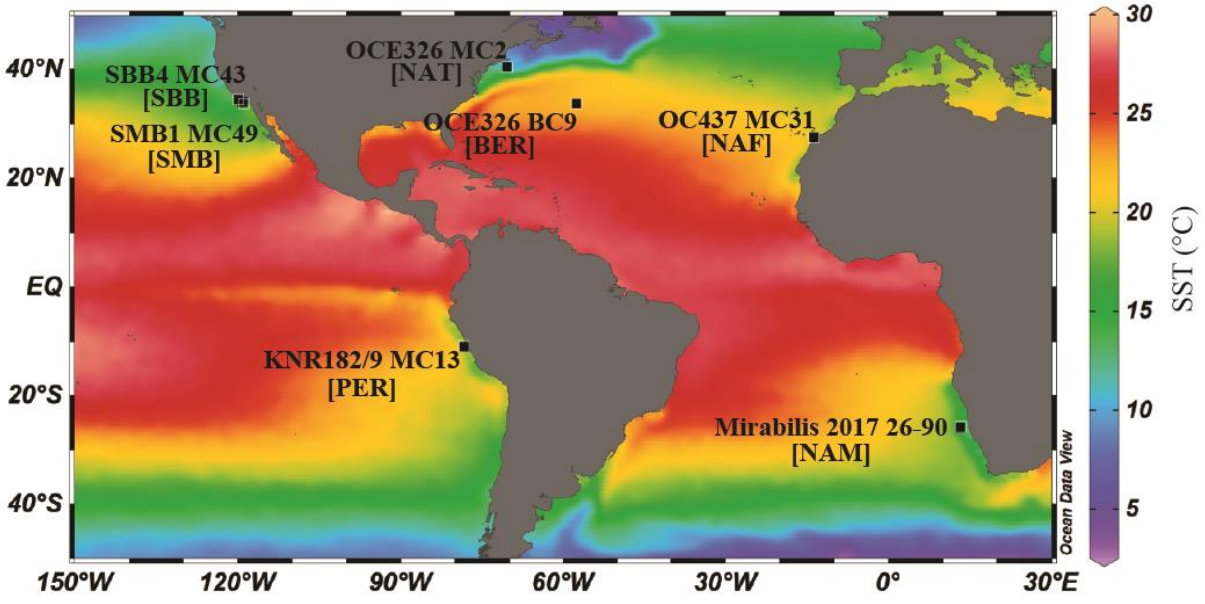

Figure 1. Sample location and annual mean SST from the WOA18 product [*Locarnini et al.*, 2019] plotted with the Ocean Data View (ODV) software [*Schlitzer*, 2021]. Acronyms for each site used in the main text are given within brackets.

Sediment cores were split onboard every 1 cm and stored at -20°C at the Biogeoscience Group ETH Zurich Sample Repository. For each core, samples from the upper 5 cm (Table 1) were freeze-dried, homogenized and fractionated by combining wet

sieving, centrifuging and tube settling protocol into four grain-size fractions: sand (>300-63 μm); coarse silt (63-10 μm ~~[CS]~~); fine silt (10-2 μm ~~[FS]~~); and clay (< 2 μm [C]), as detailed in Magill et al. [*Magill et al.*, 2018]~~Ausín et al~~.

120

Table 1. Study sites. Annual mean SST was obtained from the World Ocean Atlas (WOA18) product with a grid of 0.25°longitude by 0.25° latitude [*Locarnini et al.*, 2019] using Ocean Data View (ODV) software [*Schlitzer*, 2021]. SST errors have been propagated considering the errors provided by ODV for the selected latitudinal and longitudinal resolution. MC=multi core and BC=box core. Adopted from Ausin et al. [2021].

Study site [Acronym]	Sample name	Cruise/year	Longitude	Latitude	Water depth [m]	SST [°C]	NPP [mgC m^{-2} day^{-1}]	Depositional setting/Oxygen conditions
Peruvian margin [PER]	KNR 182/9 MC13 0-3 cm	KNR 182/9 2005	-78.17	-11.00	326	19.42±0.56	2773	Outer continental shelf/ Anoxic (OMZ impingement)
Santa Barbara Basin [SBB]	SBB4 MC43 0-2 cm	New Horizon 2001	-119.87	34.33	340	15.28±0.53	1172	Lower flank of the basin/ Sub-oxic (OMZ impingement)
Santa Monica Basin [SMB]	SMB1 MC49 1-2 cm	New Horizon 2001	-119.22	33.90	765	16.13±0.71	1055	Slightly sloping basin floor/ Anoxic (OMZ impingement)
NW Atlantic margin [NAT]	OCE326 MC2 0-3 cm	Bermuda Rise 1998	-70.54	40.46	80	12.75±1.01	1276	Shelf depocenter/ Oxic

Namibian margin [NAM]	2017 26-90 0-3 cm	Mirabilis May 2016	13.3	-26	1277	16.23±0.01	1431	Mid-slope/ Oxic
Bermuda Rise [BER]	OCE326 BC9 2-5 cm	Bermuda Rise 1998	-57.61	33.69	4517	22.51±0.27	374	Drift deposit/ Oxic
NW African margin [NAF]	OC437 MC31 0-3 cm	Cheeta Cruise 2007	-13.74	27.54	1090	19.77±0.33	1377	Upper continental slope/ Oxic

2.2. Alkenone extraction and quantification

An aliquot of 0.5-30 g of dry sediment from bulk and each grain-size fraction was used for total lipid extraction with MeOH/CH_2Cl_2 (9:1, v/v) using an EDGE® automated extraction system. Resulting total lipid extracts were saponified with 0.5M KOH/MeOH prior liquid-liquid extraction of the neutral fraction with hexane. Silica gel column chromatography was applied to separate the neutral fraction into three fractions of increasing polarity (F_1 – F_3) using hexane, CH_2Cl_2, and CH_2Cl_2/MeOH (1:1 v/v), respectively. F_2 fractions, containing the alkenones, were analysed by gas chromatography with flame ionization detection (GC-FID) to determine alkenone $C_{37:2}$ and $C_{37:3}$ concentrations using two coupled 60 m long VF-5MS columns (0.25 mm diameter, 0.25 µm phase thickness). An in-house alkenone standard was used for compound identification whereas *n*-hexatriacontane was used as external quantification standard. Analytical precision (1σ) of $U^{k'}_{37}$ was better than 0.003 units determined from replicate measurements of the in-house alkenone standard. Two 60 m long VF-5MS columns (0.25 mm diameter, 0.25um phase thickness) Corresponding $U^{k'}_{37}$ ratios were calculated according to equation (1) by Prahl and Wakeham [1987] and transformed to SST values using the calibration of Prahl et al. [1988]. Corresponding SST propagated error is 0.51 °C and considers both the analytical precision of SST measurements and the 1 σ calibration error of 0.50 °C reported by Prahl et al. [1988].

2.3. Alkenone radiocarbon analyses

The ketone fractions used for determination of alkenone concentration and unsaturation were further purified for compound specific ^{14}C analysis following Ohkouchi et al. [2005], with purity of isolated alkenone fractions assessed via GC-FID. Only

samples with a purity >90% were considered. Purified samples were subsequently transferred into tin elemental analyzer (EA) capsules with CH_2Cl_2 (3 ×50µL). The solvent was removed on a hot plate at 35°C prior wrapping the samples. Blanks were prepared in the same fashion as the samples and spiked with varying masses of oxalic acid II (OXAII; modern ^{14}C age; $\Delta^{14}C$ 1.34 ‰) and phthalic anhydride (PHA; infinite ^{14}C age; $\Delta^{14}C$ 0 ‰) reference standards in order to quantify and characterize contamination introduced during sample preparation. Samples, spiked blanks, and solvent and capsule blanks were measured within 20 h of preparation as CO_2 using an EA system interface coupled to a gas ion source (GIS)-equipped Minicarbon Dating System (MICADAS) [*McIntyre et al.*, 2016; *Synal et al.*, 2007] at the Laboratory of Ion Beam Physics, ETH Zürich. Data assessment was performed with the BATS data reduction software [*Wacker et al.*, 2010]. The model by Hanke et al. [2017] was applied to correct for constant contamination. The estimated mass of extraneous carbon was 1.12 ±0.22 µg C with $F^{14}C$ value of 0.99 ±0.2.

3. Results

3.1. Alkenone concentration and distribution

The fraction-weighted alkenone concentration is comparable to bulk values in PER, NAF, NAM, BER and SMB samples (Table 2), implying a 100-88% alkenone recovery. The large discrepancy between bulk and fraction-weighted alkenone concentrations in SBB and NAT suggests significant loss of alkenones occurred during sediment fractionation in SBB (fraction-weighted values < bulk values) and during manual column chromatography of bulk sediments in NAT due to total lipid loss during column loading (fraction-weighted values > bulk values). Alkenone concentrations in bulk sediments are highest in PER (17898 ng gdw^{-1}), and decrease in the order NAM > SMB > SBB > NAT > NAF, with minimum values in BER (28 ng gdw^{-1}; Fig. 2A and Table 2). ~~With the exception of~~Except for NAF and BER sediments, where the clay fraction hosts the largest proportion of alkenones followed by ~~FS~~fine silt, alkenone concentrations are highest within the ~~FS~~fine silt fraction at all sites. Alkenone concentrations normalized to $OC_{\%}$ also show that the OC in the smallest grain sizes (~~FS~~fine silt and ~~Clay~~clay) are associated with the highest alkenone abundances (Fig. 2B).

Table 2. Alkenone concentration and derived SST values and abundance weighted concentration and SST. Total ~~O~~organic ~~C~~carbon (TOC) and fractional abundance of grain-size fractions from bulk sediments ($Bulk_{\%}$) are taken from ~~Ausin~~ Ausín et al. [2021]. Analytical precision of $U^{k'}_{37}$ is 0.003 units. $U^{k'}_{37}$-SST propagated error is ±0.51°C.

Site	Sample	$C_{37:3}$ [ng/g]	$C_{37:2}$ [ng/g]	Alkenone concentration	Abundance weighted average	$U^{k'}_{37}$	$U^{k'}_{37}$-SST [°C]	Abundance weighted average SST [°C]	TOC [wt%]	Alkenones normalize	$Bulk_{\%}$ [%]

				[ng/gdw]	concentration [ng/gdw]					d to TOC [ng/gOC]	
PER	Bulk	3985	13914	17898	17905	0.78	21.72	22.05	13.19	108642	
	Sand	617	2649	3266		0.81	22.70		7.55	43259	0.2
	Coarse silt	2684	9163	11847		0.77	21.60		9.09	130325	38.6
	Fine silt	5551	21963	27514		0.80	22.33		17.52	157045	48.4
	Clay	31	122	153		0.80	22.36		5.21	2940	12.8
SBB	Bulk	877	1028	1905	899	0.54	14.72	13.85	2.34	81391	
	Sand	618	770	1389		0.55	15.17		3.32	41823	2.6
	Coarse silt	112	110	222		0.50	13.41		1.09	20391	63.6
	Fine silt	1038	1269	2306		0.55	15.03		3.47	66462	27.2
	Clay	762	676	1438		0.47	12.68		1.90	75699	6.7
SMB	Bulk	1245	1654	2899	2596	0.57	15.64	15.18	2.20	129671	
	Sand	2014	2823	4837		0.58	16.02		2.55	188023	2.7
	Coarse silt	54	63	117		0.54	14.61		1.08	19884	56.9
	Fine silt	2860	4096	6956		0.59	16.17		3.00	224523	32.0
	Clay	916	1115	2031		0.55	15.00		0.77	266302	8.3
NAT	Bulk	347	467	814	2548	0.57	15.74	14.30	1.03	72140	

	Sand	45	96	141		0.68	18.90		0.33	39820	11.2
	Coarse silt	87	95	182		0.52	14.17		0.65	n/d	47.6
	Fine silt	3792	3583	7375		0.49	13.14		2.43	287564	31.0
	Clay	793	775	1568		0.49	13.38		2.47	163044	10.3
NAM	Bulk	2921	4728	7649	8217	0.62	17.03	16.62	6.27	67612	
	Sand	4228	7735	11963		0.65	17.87		5.41	313734	10.7
	Coarse silt	2547	3826	6373		0.60	16.51		5.85	157689	68.5
	Fine silt	6122	9156	15278		0.60	16.48		6.98	317896	16.8
	Clay	57	78	135		0.58	15.80		4.03	1869	4.0
BER	Bulk	11	17	28	26	0.60	16.37	20.23	0.42	6751	
	Sand	n/d	n/d	n/d		n/d	n/d		0.32	n/d	5.5
	Coarse silt	3	6	9		0.69	19.02		0.12	7340	49.2
	Fine silt	9	13	22		0.59	16.15		0.47	4582	33.4
	Clay	10	113	123		0.92	25.77		0.50	0	11.9
NAF	Bulk	197	537	734	723	0.73	20.38	20.45	0.85	48976	
	Sand	272	278	549		0.51	13.72		0.63	49219	4.9
	Coarse silt	143	421	564		0.75	20.80		0.53	59259	49.1
	Fine silt	174	510	684		0.75	20.78		1.30	29389	35.6
	Clay	421	1256	1677		0.75	20.88		1.39	69135	10.5

The relative proportion of the di- and tri- unsaturated alkenones exhibit significant variability among grain size fractions at each site (Figs. 2C and D). With the exception of NAF, the proportion of alkenone $C_{37:3}$ is lower in the sand fraction in relation to the bulk in all samples, while no other clear distributional pattern is observed among size classes.

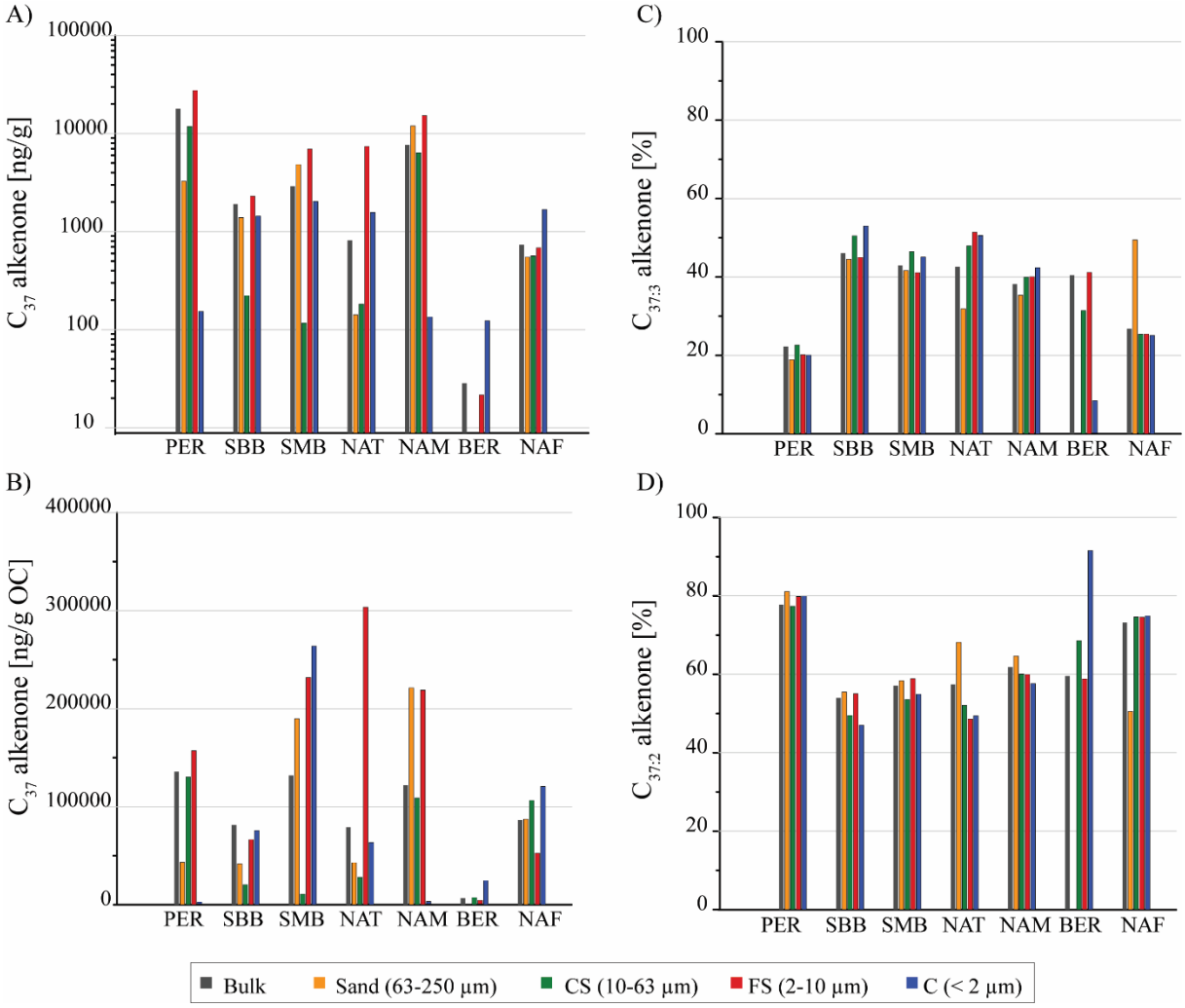
A)
100000
10000
1000
100
10
C_{37} alkenone [ng/g]
PER SBB SMB NAT NAM BER NAF
B)
400000
300000
200000
100000
0
C_{37} alkenone [ng/g OC]
PER SBB SMB NAT NAM BER NAF
C)
100
80
60
40
20
0
$C_{37:3}$ alkenone [%]
PER SBB SMB NAT NAM BER NAF
D)
100
80
60
40
20
0
$C_{37:2}$ alkenone [%]
PER SBB SMB NAT NAM BER NAF
Bulk
Sand (63-250 µm)
CS (10-63 µm)
FS (2-10 µm)
C (< 2 µm)

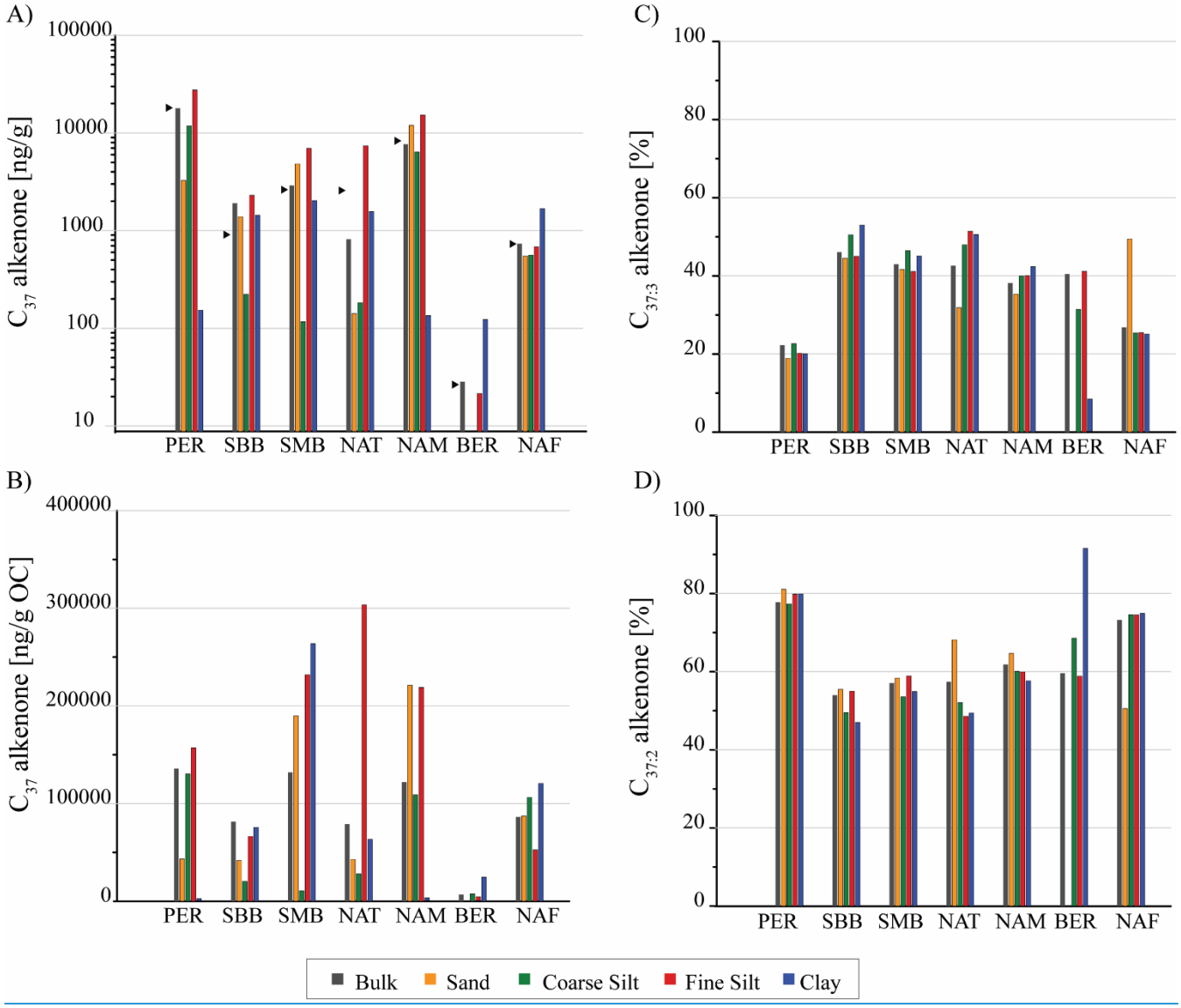

Figure 2. Alkenone concentration in bulk sediment and size fractions. A) Total C_{37} alkenone amount per gram of sediment~~,~~. Abundance weighted average concentration is indicated by black triangles, B) Total C_{37} alkenone amount normalized to $OC_{\%}$, C) $C_{37:3}$ alkenone relative amount, and D) $C_{37:2}$ alkenone relative amount. No sand fraction was available at BER.

3.2. Alkenone radiocarbon ages

The sufficient amount and purity of alkenones for ^{14}C dating was only achieved in bulk sediments and some fractions of PER, SMB, NAT and NAM ~~Alkenone ^{14}C ages in bulk sediments were measured in four samples (PER, SMB, NAT, and NAM)~~ (Fig. 3 and Table 3). Alkenone ages vary among sites, ranging from 2300 ^{14}C yr in NAM to 500 ^{14}C yr in PER. Comparison

of these results with bulk OC and planktic foraminifera ^{14}C ages from the same samples [*Ausín et al.*, 2021] shows alkenones and OC ages are comparable, and both are older than corresponding planktic foraminifera ^{14}C ages.

Table 3. ~~Alkenone radiocarbon~~ Radiocarbon ~~analysis~~analyses of alkenones extracted from bulk and grain-size fractions. Measured mass, raw and corrected fraction modern ($F^{14}C$), corrected radiocarbon ages and corresponding 1σ errors. Radiocarbon ages and associated 1σ uncertainties have been rounded according to convention.

Lab code	Site	Sample	Mass (ug C)	Raw $F^{14}C \pm 1\sigma$	Corrected $F^{14}C \pm 1\sigma$	Radiocarbon age (^{14}C yr BP) ±1σ
ETH-	PER	Bulk	46	0.9402 ±0.0070	0.9402 ±0.0089	490 ±75
95663.1.1	PER	~~CS~~Coarse silt	78	0.9300 ±0.0169	0.9300 ±0.0074	580 ±65
95664.1.1	PER	Fine silt~~FS~~	59	0.9473 ±0.0045	0.9473 ±0.0080	4310 ±70
95665.1.1	SMB	Bulk	56	0.9271 ±0.0048	0.9271 ±0.0091	610 ±80
95666.1.1	SMB	Sand	68	0.7345 ±0.0065	0.7345 ±0.0068	2480 ±75
95667.1.1	SMB	Fine silt~~FS~~	86	0.8618 ±0.0029	0.8618 ±0.0074	1190 ±70
95668.1.1	SMB	Clay	27	0.6830 ±0.0033	0.6830 ±0.0094	3060 ±110
95669.1.1	NAT	Bulk	51	0.8623 ±0.0034	0.8623 ±0.0080	1190 ±75
95670.1.1	NAT	Sand	30	0.6812 ±0.0025	0.6812 ±0.0123	3080 ±150
95671.1.1	NAT	Fine silt~~FS~~	91	0.8344 ±0.0025	0.8344 ±0.0077	1450 ±75
95672.1.1	NAM	Bulk	66	0.7436 ±0.0023	0.7436 ±0.0069	2380 ±75
95673.1.1	NAM	Sand	47	0.6993 ±0.0021	0.6993 ±0.0066	2870 ±75
95674.1.1	NAM	Coarse silt~~CS~~	48	0.7692 ±0.0023	0.7691 ±0.0069	2110 ±70
95675.1.1	NAM	~~FS~~Fine silt	107	0.7108 ±0.0050	0.7108 ±0.0060	2740 ±70

Purification of alkenones for radiocarbon dating was possible in some of the size fractions for these four samples. Alkenones contained in sand fractions are the oldest, while those hosted within ~~FS~~fine silt and ~~CS~~coarse silt show the smallest age offsets with respect to bulk sediments (Fig. 4).

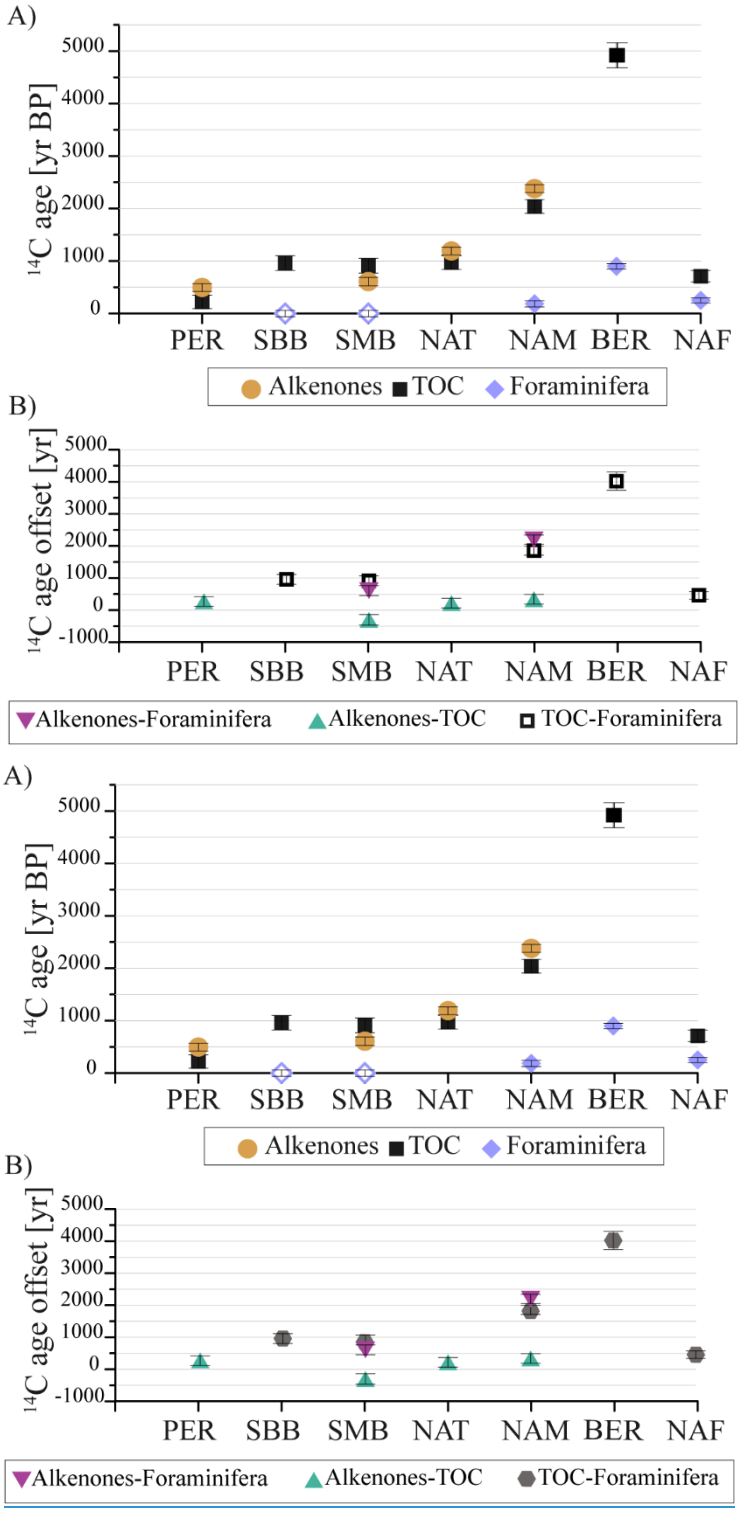
A)
^{14}C age [yr BP]
5000
4000
3000
2000
1000
0
PER SBB SMB NAT NAM BER NAF
Alkenones TOC Foraminifera
B)
^{14}C age offset [yr]
5000
4000
3000
2000
1000
0
-1000
PER SBB SMB NAT NAM BER NAF
Alkenones-Foraminifera Alkenones-TOC TOC-Foraminifera
A)
^{14}C age [yr BP]
5000
4000
3000
2000
1000
0
PER SBB SMB NAT NAM BER NAF
Alkenones TOC Foraminifera
B)
^{14}C age offset [yr]
5000
4000
3000
2000
1000
0
-1000
PER SBB SMB NAT NAM BER NAF
Alkenones-Foraminifera Alkenones-TOC TOC-Foraminifera

205

Figure 3. Radiocarbon ages of alkenones (this study), TOC and planktic foraminifera [*Ausín et al.*, 2021] from bulk sediment samples (A) and age discrepancies among them (B). Open diamonds indicate foraminifera that incorporate bomb ^{14}C.

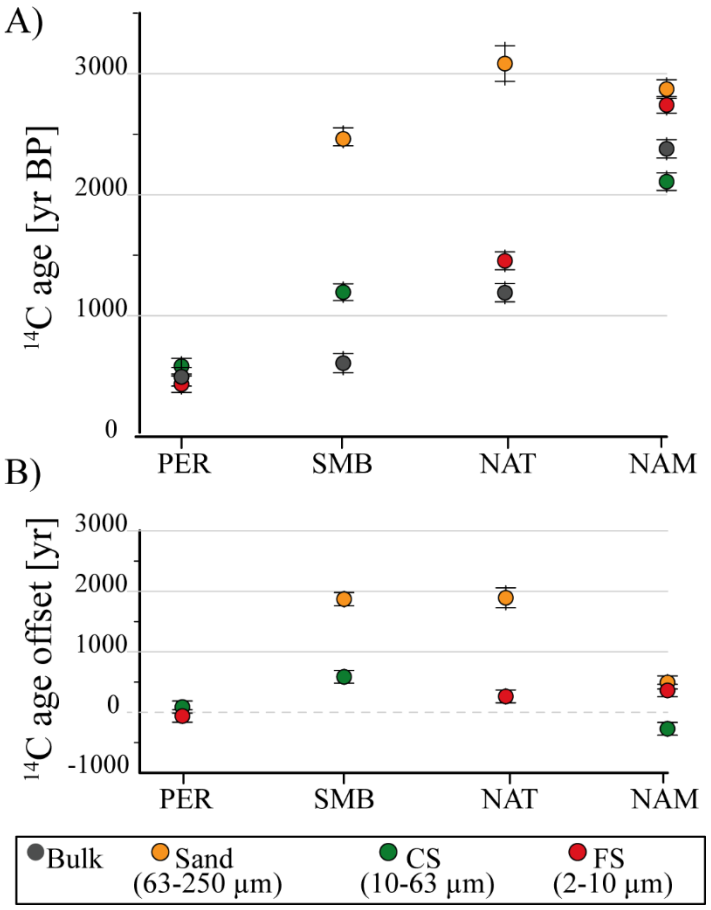
A)
3000
2000
1000
0
^{14}C age [yr BP]
PER
SMB
NAT
NAM
B)
3000
2000
1000
0
-1000
^{14}C age offset [yr]
PER
SMB
NAT
NAM
Bulk
Sand (63-250 µm)
CS (10-63 µm)
FS (2-10 µm)

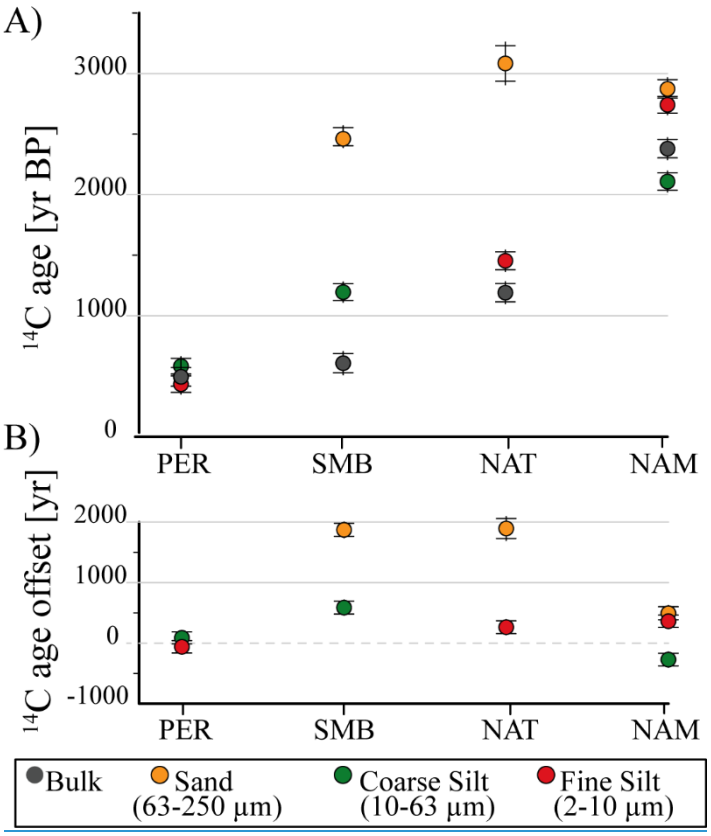

Figure 4. Radiocarbon ages of alkenones contained in bulk and grain-size fractions at each study site (A) and age discrepancies between ^{14}C ages of alkenones in size fractions and corresponding bulk sediment (B).

3.3. Alkenone-SST

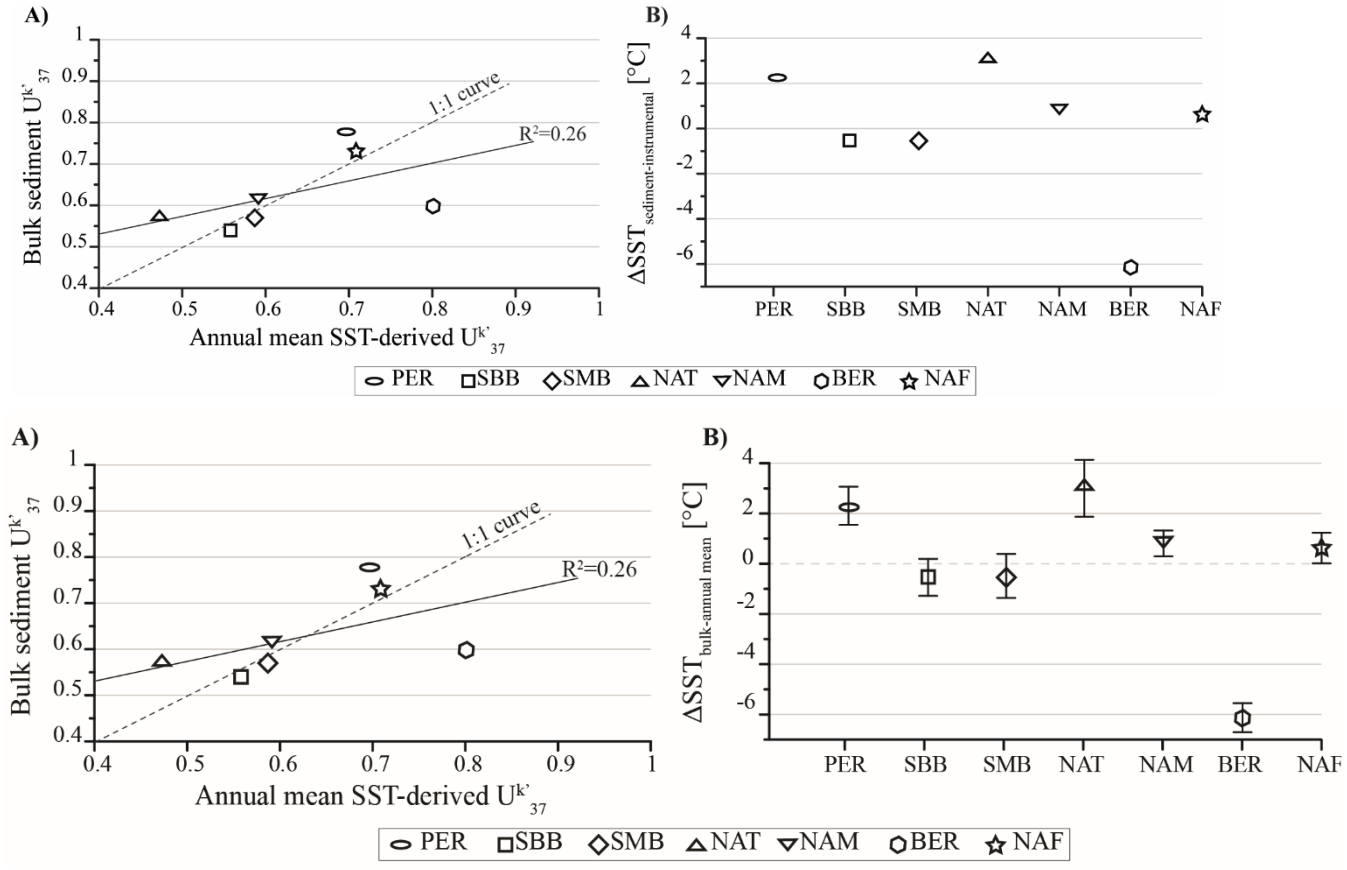

Figure 5. SST from bulk sediments and atlas data (annual mean) [*Locarnini et al.*, 2019]. A) $U^{k'}_{37}$ ratio from bulk core-top sediments compared to $U^{k'}_{37}$ ratio calculated from atlas annual mean SST [*Locarnini et al.*, 2019]. B) Comparison of SST from bulk sediments and atlas annual mean SST and propagated errors.~~,~~

$U^{k'}_{37}$ ratios and corresponding alkenone-SST values from bulk sediments show a weak positive relationship with annual-mean SST observations (R^2=0.26) (Figs. 5A). ~~Only~~ Sediment and atlas SST values from ~~samples from~~ SBB~~,~~, ~~and~~ SMB and NAF ~~, NAM and NAF are comparable to atlas data~~fall within the associated uncertainties ~~,~~whereas temperature differences ranging from -6±0.6°C to +3±1.1°C ~~are observed at the other sites~~PER, NAT, NAM and BER (Fig. 5B). Abundance-weighted average SST of the analyzed grain-size fractions compares relatively well with bulk SST except at BER (Table 2), which shows a -4.4°C difference. The latter is attributed to the lack of detectable alkenones in the sand fraction of BER. ~~Except for BER,~~ SST discrepancies imply core-top SST is significantly warmer than surface water temperature at PER and NAT. $U^{k'}_{37}$-SST shows significant variability among size grain size fractions at each site (Fig. 6A). The smallest SST variation among size fractions is observed at PER, SMB and NAM. Sand shows the warmest temperature signal in relation to other fractions at 5 out of 6 locations (Fig. 6). ~~Overall~~Except for PER and NAT, ~~FS~~fine silt shows the smallest temperature offsets with bulk sediment at each site (Fig. 6B). No specific fraction shows larger/smaller offsets with annual averaged SST (Fig. 6C).

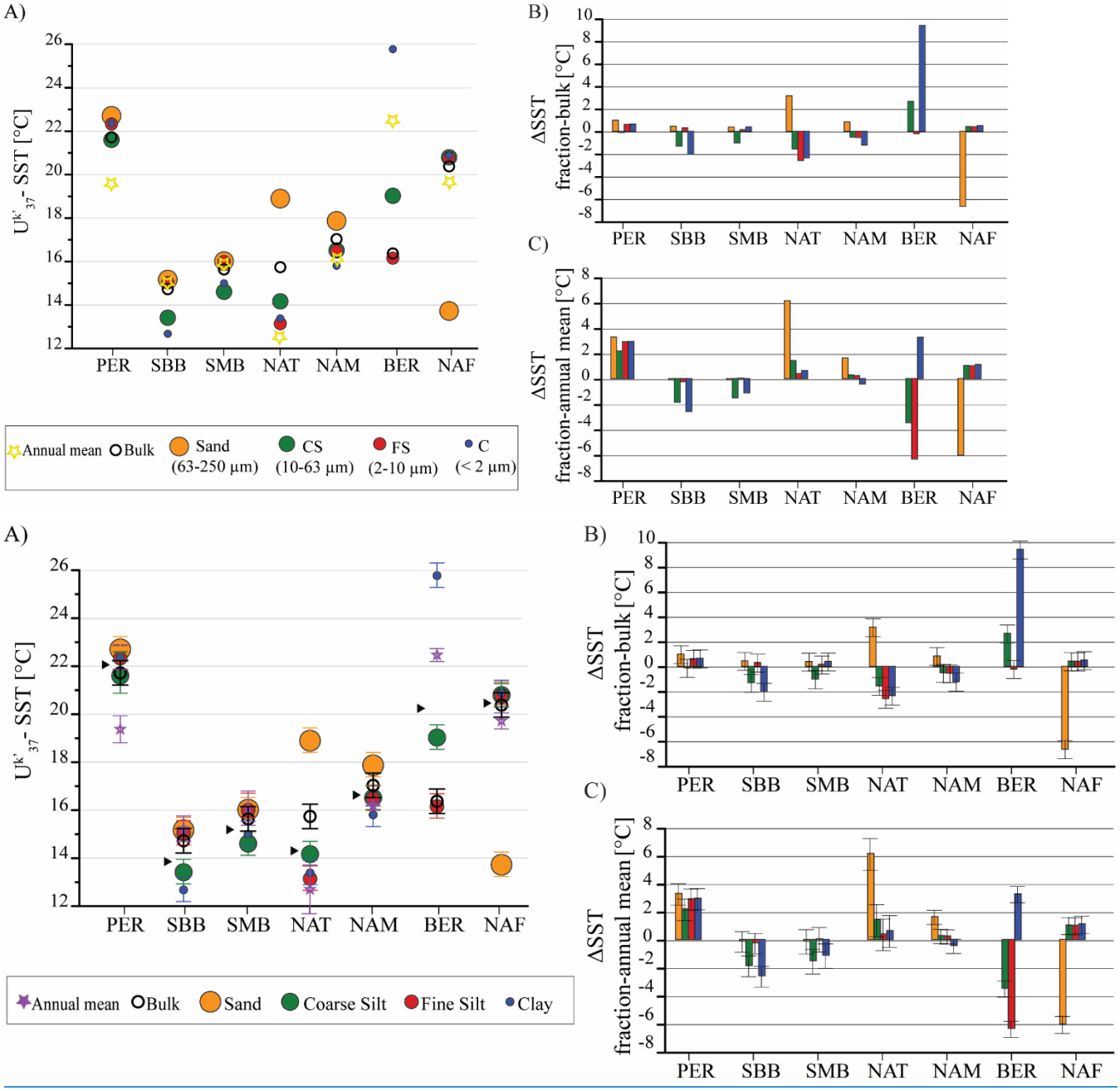

Figure 6. SST at each site. A) Bulk-, grain-size, and annual mean SST [*Locarnini et al.*, 2019]. Abundance weighted average SST is indicated by black triangles. Temperature difference between B) each grain-size fraction and bulk- SST ~~bulk- and annual mean SST~~ and C) bulk- and annual mean SST~~each grain-size fraction and bulk- SST~~.

4. Discussion

4.1. Alkenone signals (and biases) from bulk sediment samples

Alkenone concentrations in bulk sediments follow the identical pattern to that of $OC_{\%}$ (R^2=0.99, n=7), indicating similar preservation mechanisms for both and that bulk OC is predominantly derived from marine primary production at each location (Fig. 7A). These results support the hypothesis that alkenone fate in marine sediments is largely influenced by organo-mineral relationships and hydrodynamic mechanisms [*Ausín et al.*, 2021].

Older-than-foraminifera alkenone ages indicate contributions of pre-aged alkenones in the four samples analyzed (Fig. 3), and previously observed at the three other studied regions: Santa Barbara Basin, Bermuda Rise, and, to a lesser extent, NW African margin [*Gesine Mollenhauer and Eglinton*, 2007; *Nao Ohkouchi et al.*, 2002]. These results imply that alkenone signatures are influenced by processes such as bioturbation, preferential degradation of fresh alkenones, and/or translocation of older alkenones (e.g., lateral advection via entrainment in sediment resuspension-deposition cycles or nepheloid layers) associated with along- or across-margin transport. A significant influence from bioturbation is unlikely since all sites are characterized by high sedimentation rates (>20 cm/kyr) [*Balestra et al.*, 2018; *Bothner et al.*, 1981; *Inthorn et al.*, 2006b; *Gesine Mollenhauer et al.*, 2005; *Nao Ohkouchi et al.*, 2002; *Schaaf and Thurow*, 1995; *Wefer et al.*, 1990], and given that some sites (e.g., SMB) contain varved sediments deposited under the influence of anoxic or sub-oxic bottom waters. In contrast, prolonged particle aging due to resuspension and downslope transport is a feature of OC-rich continental margin sediments [*Gesine Mollenhauer et al.*, 2008]. The joint assessment of ^{14}C ages and SSTs among grain-size sediment fractions at each site provides insights into the influence of selective degradation and alkenone translocation mechanisms (Secs. 4.3. and 4.4).

Older alkenones may carry a different temperature signal than that of the water column overlying the depositional site if they originate from a distal location or were synthesized during colder/warmer past periods. Alkenones from Santa Monica and Santa Barbara basins and the North African margin ~~SMB and, SBB and NAF~~ are found to ~~accurately~~ reflect local instrumental SST within associated errors (Fig. 5), while a positive discrepancy ranging from ~~+1~~0.8±0.5°C to ~~-3~~3±1.1 °C ~~discrepancy~~ (towards warmer temperatures) is observed at other locations with the exception of BER (-6 °C±0.6°C). In both cases, these temperature discrepancies exceed the analytical uncertainty. Such a ~~warmer bias~~warm bias is a common feature of sediments from many locations with the exception of those underlying tropical waters [*Conte et al.*, 2006; *F. G. Prahl et al.*, 2010]. Previous ~~authors~~ works ~~argue~~ indicate that this bias cannot be solely explained by faster degradation of the more-unsaturated $C_{37:3}$ alkenone [*Rosell-Melé et al.*, 1995] and ascribe it to seasonal production and/or lateral transport of alkenones [*Conte et al.*, 2006; *Goñi et al.*, 2001; *Sachs and Anderson*, 2003]. ~~With respect to~~ The large and cold bias observed at ~~BER~~Bermuda Rise, ~~we used~~ could be due to the use of sub-surface sediments (2-5 cm; foraminifera ^{14}C age=900±50 yr) rather than surface sediments. Nevertheless, ~~but~~ alkenone-SST from the core-top (0-1 cm) of the exact same core [*Nao Ohkouchi et al.*, 2002] also leads to a -6.6°C (cold) bias. Recent evidence on the advection of lithogenic particles from the shelf of the NE Canadian maritime provinces (Nova Scotia, Newfoundland) supports lateral transport of alkenones from these colder and more

productive waters, previously proposed to explain hydrogen isotope and ^{14}C-depleted values of alkenones at this site [*Englebrecht and Sachs*, 2005; *Hwang et al.*, 2021; *Nao Ohkouchi et al.*, 2002], and consistent with the cold bias found at BERBermuda Rise.

In light of the strong agreement between $OC_{\%}$ and alkenone concentration and the temporal and temperature biases observed in bulk surface sediments from all the studied sites, we speculate that alkenone-proxy signals from continental margin sediments can be strongly modulated by the interplay between organo-mineral relationships and differential hydrodynamic sorting of mineral particle sizes. Alkenone concentrations, ^{14}C ages and $U^{k'}_{37}$-SST values measured on specific grain-size fractions provide a means to evaluate this hypothesis.

4.2. Influence of hydrodynamic sorting processes on sedimentary alkenone signals

Despite evidence of substantial alkenone loss during sample workup in one or several size fractions from SBB and bulk sediments from NAT, the overall strong positive correlation between alkenone concentration and $OC_{\%}$ in bulk sediments (R^2=0.99) and sediment fractions (R^2=0.81) indicates mutual preservation mechanisms also exist within mineral grain size classes (Fig. 7A). Hence, and as observed for OC [*Ausín et al.*, 2021], the large differences in alkenone concentration among grain size fractions correspond to preferential association with, and protection by mineral grains having greater surface area (i.e., FSfine silt) [*Richard G. Keil et al.*, 1994a; *Richard G. Keil et al.*, 1994b; *Premuzic et al.*, 1982] and to further exposure to degradation for alkenones (and associated organic matter) residing in the least-cohesive grain size fraction that is more prone to resuspension (i.e., CScoarse silt) [*McCave and Hall*, 2006b; *McCave et al.*, 1995].

When alkenone concentrations in size fractions are normalized to the bulk sediment mass, the primary contribution of FSfine silt — and CScoarse silt to a lesser extent — is apparent (Fig. 7B). Given the propensity of FSfine silt to resuspension and mobilization under strong currents [*McCave and Hall*, 2006b], we argue that the temporal offsets and temperature biases observed in bulk sediments can be largely ascribed to the lateral supply of pre-aged/allochthonous alkenones sorbed onto the surfaces of fine-grained, mobilizable (fine-silt) minerals. To a lesser extent, advection of coarser grains (i.e., CScoarse silt) can also contribute significantly to signals embedded in bulk sediments. Consistent with this notion, FSfine silt shows the smallest age and temperature offset with respect to corresponding bulk sediments (Fig. 4B and 6B). In addition to SST and temporal offsets, our results suggest that the alkenone-based productivity proxy [*Raja and Rosell-Melé*, 2021] may also be influenced by the translocation and deposition of fine sediments from distal regions. Its impact can be particularly relevant in regions where the contribution of silt minerals to the bulk sediment mass is significant.

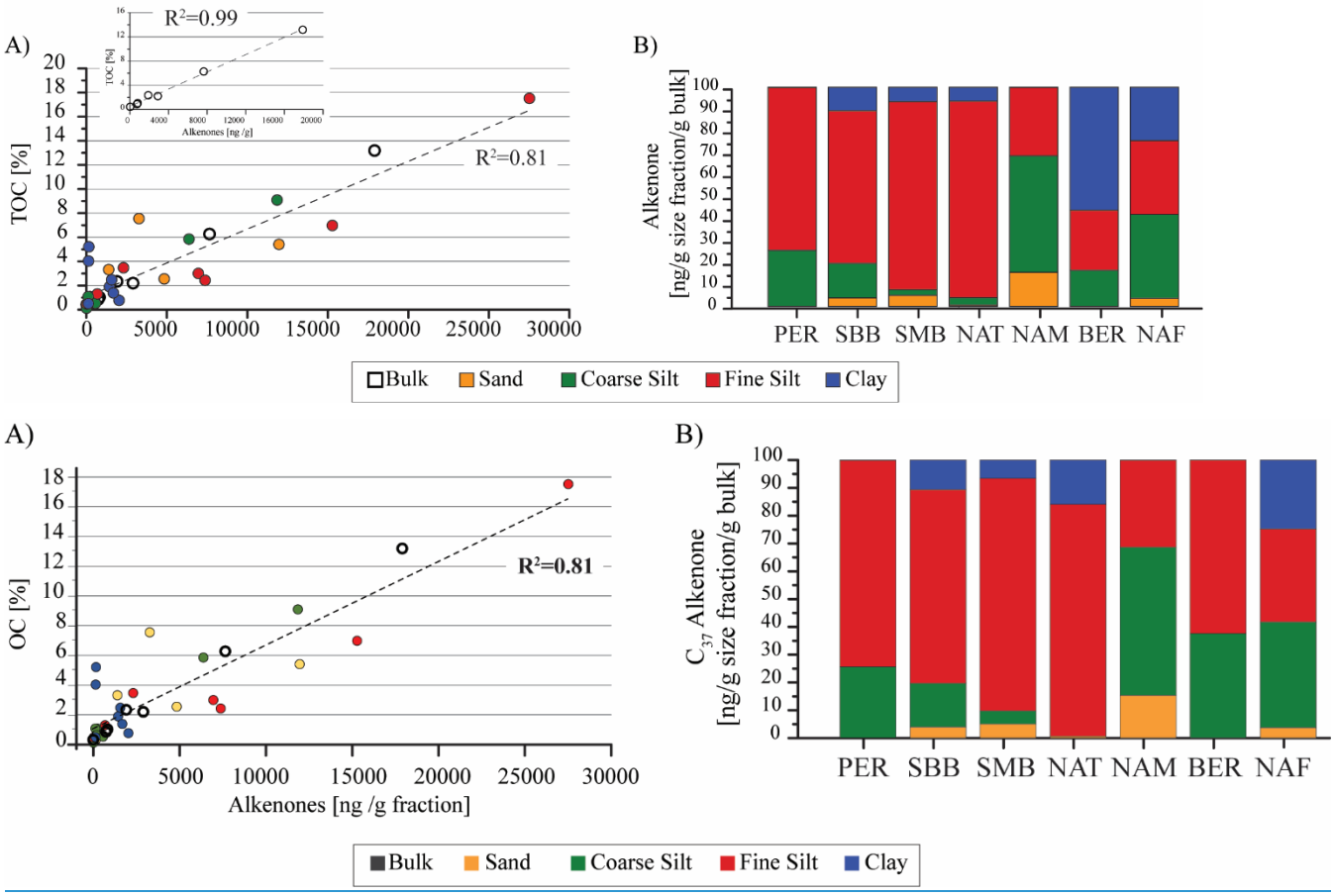

Figure 7. Alkenone correlation with $OC_{\%}$ from Ausín et al. [2021] in bulk sediments ~~(upper left panel)~~ and grain size fractions (A) and within each size fraction per gram of bulk sediment (B).

4.3. Selective alkenone degradation during lateral particle transport

The strong grain-size dependence of OC-^{14}C ages found in all the study sites [*Ausín et al.*, 2021] is not uniformly observed for the more limited alkenone-^{14}C age data set (Fig. 4). Yet, the strong positive linear relationship observed between ~~both~~ the ^{14}C ages of both types of organic matter (R^2=0.78) suggests alkenones could exhibit a similar age-grain-size relationship driven by the differential influence of hydrodynamic processes on mineral grain sizes (Fig. 8). Considering associated uncertainties, only samples ~~at~~ from the Peruvian, North Atlantic and Namibian margins ~~PER, NAT and NAM~~ show warmer-than-instrumental alkenone-derived SST~~Overall, FS and sand show warmer than instrumental alkenone derived SSTs at most sites (Fig. 6C)~~, with the sand fraction exhibiting the greatest warm bias and oldest ages. These results may reflect extensive diagenetic alteration as a consequence of two non-exclusive mechanisms: i) input of pre-aged alkenones synthesized in warmer waters, or ii) selective microbial or abiotic oxidative degradation of more labile (fresher) polyunsaturated ($C_{37:3}$) alkenones as

a consequence of decreasing mineral protection with increasing grain size. Although there has been evidence for [*Gong and Hollander*, 1997; *Hoefs et al.*, 1998] and against [*Grimalt et al.*, 2000; *Sikes et al.*, 1991; *Teece et al.*, 1998] the impact of selective alkenone degradation on sediment $U^{k'}_{37}$ ratios, more recent work has demonstrated that autoxidation and aerobic bacterial degradation can cause selective degradation of more unsaturated alkenones, altering corresponding $U^{k'}_{37}$ ratios, resulting in warm temperature biases of up to 5.9 °C [*Rontani et al.*, 2013, and references therein]. Given that the relative increase of SST and ^{14}C age is most pronounced for the [comparatively immobile] sand fraction, and that it is difficult to envision how advected alkenones systematically carry a warmer signal than that of the overlying water column for diverse locations, we suggest that selective degradation of $C_{37:3}$ provides the most viable explanation. While further evidence is required in order to attribute ~~warmer bias~~warm biases to selective degradation of $C_{37:3}$ within specific size fractions, a universal SST-grain size relationship is not expected because corresponding SST depends on the temperature of surface waters where alkenones were produced. In this context, a much colder initial surface ocean signal than that at the depositional location could mask the influence of selective degradation during oxic transport.

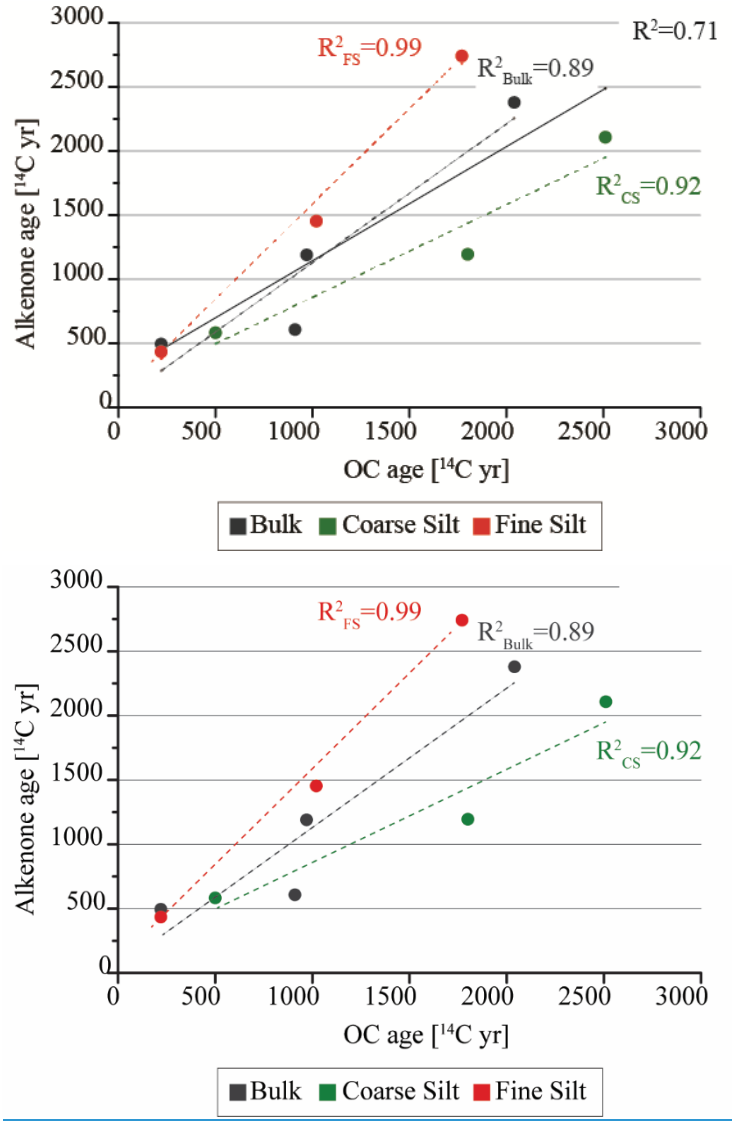

Figure 8. Relationship between OC- [*Ausín et al.*, 2021] and alkenone- ^{14}C ages. ~~The black solid regression line considers all the data (n=10; R^2=0.71).~~

335

4.4. Site-specific hydrodynamic mechanisms

The selected sites largely vary with respect to primary productivity, oxic conditions and water depth, spanning a range of hydrographic and depositional settings comparable to those selected for paleoceanographic investigations. Alkenone ages from

340 all PER grain size fractions are similar and close to modern values (Fig. 4). This observation, along with the largest alkenone concentrations, are attributed to the high vertical flux of fresh OM [*Reimers and Suess*, 1983] and agree with a minor, although

discernable, effect of hydrodynamic sorting on OC signals [*Ausín et al.*, 2021]. Alkenone-derived SST values of size fractions and bulk sediments at PER are similar, but differ markedly from (are 2.3°C warmer than) instrumental SST (Fig. 6) [*Kienast et al.*, 2012; *F. G. Prahl et al.*, 2010]. Resuspension of recently deposited bottom sediments from the shelf and offshore transport as suggested by Pak et al. [1980] to explain particle advection maxima at 140-200 m water depth at this location is discarded because across-shelf transport would hypothetically translocate a colder signal. Selective degradation of $C_{37:3}$ seems unlikely, as this is expected to exert a differential impact on the $U^{k'}_{37}$ of the different fractions based on their size (i.e., propensity for resuspension and OM exposure to oxic conditions during transport) and mineral surface area (i.e., potential for OM protection), whereas our results show comparable $U^{k'}_{37}$ for all fractions. Prior authors [*Kienast et al.*, 2012; *Rein et al.*, 2005] speculated sedimentary C_{37} alkenones at this location are skewed towards El Niño events arguing coccolithophores preferentially grow in oligotrophic waters. In fact, while coccolithophores generally dominate the phytoplankton community in oligotrophic waters their absolute abundance is highest in high-nutrient periods/regimes [e.g., *Flores and Sierro*, 2007]. Alkenone producers *E. huxleyi* and *G. oceanica* are generally linked to eutrophic waters and periods of maximum primary productivity [*Tyrrell and Merico*, 2004]. Recent work reveals a significant positive correlation between C_{37} alkenone concentrations from a global surface sediment compilation and maxima Chl*a* in overlying waters [*Raja and Rosell-Melé*, 2021]. Accordingly, we suggest preferential alkenone production during the austral summer [*F. G. Prahl et al.*, 2010], when surface waters are warmest and primary productivity is at its highest, is the most feasible explanation for the warm bias from sedimentary alkenones observed at this location.

Alkenone ages from grain-size fractions at NAM are more dissimilar than at PER~~,~~ and are 2000-3000 ^{14}C yr older than coeval foraminifera. Moreover, alkenone-derived SST values among grain size fractions range from 15.8 °C to 17.9 °C (Figs. 4 and 6). Both sites are characterized by high productivity, low oxygen exposure and local deposition, and defined as "initial" depositional systems [*Ausín et al.*, 2021] in terms of OC dispersal and deposition. Site-specific characteristics, such as lower primary productivity and a broader shelf might favor a larger impact of hydrodynamic processes on sedimentary OC and alkenone signals at NAM. Our results suggest lateral supply of pre-aged alkenones influenced by hydrodynamic particle sorting and potentially originating from different locations on the margin, and are consistent with prior models of sediment transport by bottom and intermediate nepheloid layers leading to the formation of an upper slope OC depocenter [*Inthorn et al.*, 2006a; *Inthorn et al.*, 2006b]. However, bulk SST only differs 0.8°C±0.5°C from annual averaged SST, indicating that the apparent influence of hydrodynamic mineral sorting on sedimentary alkenone ^{14}C age and abundance might not necessarily impart an equivalent bias in alkenone temperature signals. Past changes in the temperature gradient between the sites of alkenone production and deposition may, however, lead to larger and unnoticed SST biases in the sedimentary record.

Large alkenone age and temperature discrepancies among grain-size fractions are observed in NAT (Fig. 4). NAT is located within the New England Mud Patch, where large amounts of ~~FS~~fine silt advected by strong bottom currents and storm-induced transport of sand occurs [*Goff et al.*, 2019], enhancing the oxygen exposure time of OM associated with both grain size fractions during transport. This mechanism would foster alkenone aging/input of pre-aged alkenones as well as selective degradation of $C_{37:3}$ in low-surface-area minerals, as observed for sand fractions. Sedimentary alkenones reflect a warmer signal than that of

the overlying surface water, in contrast with the colder bias observed from offshore, slope sediments [*Hwang et al.*, 2014] explained by lateral advection of resuspended sediments from a colder upstream location [*Hwang et al.*, 2009; *Hwang et al.*, 2021]. On the shelf (< 150 mwd), however, accumulation of advected fine silt sediments occurs under a west-directed transport, as shown by seismic profiles and the presence of active southwestward megaripples [*Goff et al.*, 2019; *Twichell et al.*, 1981]. Lateral transport of fine sediments to this site from the Georges Bank to the east, as hypothesized by Twichell et al. [1981], would result in the entrainment and deposition of sedimentary alkenones carrying a warmer signal.

Large alkenone age offsets are also apparent among grain-size fractions from SMB. In this basin, the impact of hydrodynamic processes is strongly modulated by basin topography and by local variability in bottom water oxygen content, which can lead to differences in alkenone ages of flank and depocenter sediments [*Gesine Mollenhauer and Eglinton*, 2007]. The ~~fidelity~~ good agreement between ~~of the~~ sediment- and instrumental-SST signature in SMB may be coincidental, as the presence of aged alkenones in all size fractions indicates addition of allochthonous (advected) material. Indeed, bomb radiocarbon was present in co-eval planktic foraminifera, whereas this was not detectable in corresponding alkenone samples. These results may imply rapid degradation of fresh alkenones and/or alkenone input from distal locations.

Conclusions

Alkenone concentration, ^{14}C age and SST was determined in surficial sediments and corresponding grain-size fractions (clay, fine and coarse silt, and sand) retrieved from 6 continental margin settings.

Our results provide clear evidence for alkenone transport as a consequence of their intimate association with surfaces of fine-grained minerals; subsequent hydrodynamic mineral sorting and associated exposure to oxic degradation during transport imparts a strong influence on sedimentary alkenone signals. Alkenones preferentially reside within the fine silt fraction (2-10 µm) of sediments. Overall, this fraction is the largest alkenone contributor to marine sedimentary signals and exerts a predominant control on the alkenone concentration, ^{14}C age and derived SST values manifested in bulk sediments. Alkenone ^{14}C ages from ~~FS~~fine silt (but also ~~CS~~coarse silt) indicate resuspension and protracted transport of alkenones from distant regions (or past time periods), suggesting that the intimate association of alkenones with fine grained sediments has important implications for the paleoreconstruction of primary productivity and SST based on alkenone concentrations and distributions.

~~Significant $U^{k'}_{37}$ SST variability is observed among grain-size fractions. We suggest that the predominantly warmer than instrumental SST may reflect two alternative processes: 1) selective degradation of the tri-unsaturated C_{37} alkenone attributed due to lower OM protection offered by larger particles under oxic conditions, and 2) systematic input of allochthonous alkenones synthesized in warmer waters. Further work is needed to determine the validity and importance of these scenarios.~~

Assessment of alkenone amount, ^{14}C age, and SST in grain-size fractions sheds important new light on processes controlling alkenone signatures in bulk sediments from the studied sites, including vertical settling of fresh material, lateral transport of allochthonous and pre-aged alkenones and alkenone degradation. The combined influence of alkenone-mineral associations and hydrodynamic particle sorting processes on sedimentary alkenone signals is discernable at all sites, ranging from almost

negligible (e.g., at PER) to substantial (e.g., BER). Yet, pronounced impacts on alkenone ^{14}C age and concentration do not necessarily impart an equivalent bias in $U^{k'}_{37}$-SST (e.g., ~~SBM~~ SMB and NAM), as the latter also depends on the temperature gradient between the sites (or time periods) of alkenone production and deposition. Past changes in this temperature gradient could, however, lead to larger SST biases in the sedimentary record. In this regard, the complementary assessment of alkenone provenance in size fractions via isotope analyses (e.g., $\delta^{13}C$ and δD in alkenones and Nd, Pb, Sr in lithogenic grains) would shed further light on particle transport pathways and the magnitude of the impact of allochthonous and asynchronous material on local proxy signals.

Our results highlight the importance of considering the joint influence of OM-mineral relationships and hydrodynamic mineral sorting processes (e.g., lateral transport) on sedimentary alkenone signatures (amount, age, and temperature) and their relationship to surface waters overlying the depositional location. Thus, multiproxy approaches combining organic and inorganic proxy records and based on proxy carriers that show different hydrodynamic behavior are essential to unravel the magnitude and pace of past rapid climate changes.

Data availability. All original data used in this study, necessary to understand, evaluate, and replicate this research, are presented and available in tables within the main text or as supplementary material.

Author contribution. B.A and T.I.E. conceived and designed this investigation. N.H. assisted with radiocarbon analyses. E.B. assisted with grain-size fractionation. B.A. prepared and processed the samples, analyzed the results, and wrote the manuscript with contributions by all coauthors.

Competing interests. The authors declare that they have no conflict of interest.

Acknowledgements

This study was supported by the project "TRAMPOLINE" (200021_175823) funded by the Swiss National Science Foundation. ~~The majority of the~~The samples included in this study were collected ~~during the following cruises: R/V *Mirabilis* 2016, R/V New Horizon 01-12 funded by the National Science Foundation grant OCE-9907129 (T. Eglinton), R/V Oceanus cruise 437-7 funded by the National Science Foundation collaborative grants OCE-0402348 (P. deMenocal) and OCE-0402533 (T. Eglinton and T. Wagner), R/V Knorr KNR-182-9 funded by the National Science Foundation grant OCE-0327226 (J. Moffett), and R/V Oceanus cruise 326. Participation of T. Eglinton in cruises R/V Knorr KNR-182-9 and R/V Oceanus cruise 326 was supported by grant OCE-0526268 (T. Eglinton) and grant OCE-9809624 (T. Eglinton and JM Hayes), respectively, by the National Science Foundation, and participation of B. Ausín in R/V *Mirabilis* 2016 was supported by grant FEL-44 15-2 from the Swiss Federal Institute of Technology in Zurich (B. Ausín). We acknowledge the Regional Graduate Network for Oceanography (RGNO) Discovery Camps, supported by the Agouron Institute, the Simons Foundation, the Scientific Committee for Oceanographic Research (SCOR), the Ministry of Fisheries and marine Resources (MFMR), the National Marine Information and Research Center (Nat MIRC), the University of Namibia (UNAM), ETH Zurich and the swiss

i-research & training institute, as well as scientists and crew of the R/V *Mirabilis* for realization of Namibian margin sampling in 2016. We are grateful to all crew members involved in sample collection, in particular to Daniel Montluçon.

References

Ausín, B., E. Bruni, N. Haghipour, C. Welte, S. M. Bernasconi, and T. I. Eglinton (2021), Controls on the abundance, provenance and age of organic carbon buried in continental margin sediments, *Earth and Planetary Science Letters*, *558*, 116759.

Ausín, B., C. Magill, N. Haghipour, Á. Fernández, L. Wacker, D. Hodell, K.-H. Baumann, and T. I. Eglinton (2019), (In)coherent multiproxy signals in marine sediments: Implications for high-resolution paleoclimate reconstruction, *Earth and Planetary Science Letters*, *515*, 38-46.

Balestra, B., N. B. Quintana Krupinski, T. Erohina, J. Fessenden-Rahn, T. Rahn, and A. Paytan (2018), Bottom-water oxygenation and environmental change in Santa Monica Basin, Southern California during the last 23kyr, *Palaeogeography, Palaeoclimatology, Palaeoecology*, *490*, 17-37.

Bao, R., C. McIntyre, M. Zhao, C. Zhu, S.-J. Kao, and T. I. Eglinton (2016), Widespread dispersal and aging of organic carbon in shallow marginal seas, *Geology*.

Bao, R., T. S. van der Voort, M. Zhao, X. Guo, D. B. Montluçon, C. McIntyre, and T. I. Eglinton (2018a), Influence of Hydrodynamic Processes on the Fate of Sedimentary Organic Matter on Continental Margins, *Global Biogeochemical Cycles*, *32*(9), 1420-1432.

Bao, R., M. Uchida, M. Zhao, N. Haghipour, D. Montlucon, A. McNichol, L. Wacker, J. M. Hayes, and T. I. Eglinton (2018b), Organic Carbon Aging During Across-Shelf Transport, *Geophysical Research Letters*, *45*(16), 8425-8434.

Bendle, J., and A. Rosell-Melé (2004), Distributions of UK37 and UK37′ in the surface waters and sediments of the Nordic Seas: Implications for paleoceanography, *Geochemistry, Geophysics, Geosystems*, *5*(11), n/a-n/a.

Benthien, A., and P. J. Müller (2000), Anomalously low alkenone temperatures caused by lateral particle and sediment transport in the Malvinas Current region, western Argentine Basin, *Deep Sea Research Part I: Oceanographic Research Papers*, *47*(12), 2369-2393.

Boon, J. J., F. W. van der Meer, P. J. W. Schuyl, J. W. de Leeuw, and P. A. Schenck (1978), Organic Geochemical analyses of core samples from site 362, Walvis Ridge, DSDP Leg 40.*Rep.*, 627–637 pp.

Bothner, M. H., E. C. Spiker, P. P. Johnson, R. R. Rendigs, and P. J. Aruscavage (1981), Geochemical evidence for modern sediment accumulation on the continental shelf off southern New England *Journal of Sedimentary Research*, *51*, 281–292.

Bröder, L., T. Tesi, A. Andersson, I. Semiletov, and Ö. Gustafsson (2018), Bounding cross-shelf transport time and degradation in Siberian-Arctic land-ocean carbon transfer, *Nature Communications*, *9*, 806.

Conte, M. H., M.-A. Sicre, C. Rühlemann, J. C. Weber, S. Schulte, D. Schulz-Bull, and T. Blanz (2006), Global temperature calibration of the alkenone unsaturation index (UK′37) in surface waters and comparison with surface sediments, *Geochemistry, Geophysics, Geosystems*, *7*(2), n/a-n/a.

Englebrecht, A. C., and J. P. Sachs (2005), Determination of sediment provenance at drift sites using hydrogen isotopes and unsaturation ratios in alkenones, *Geochimica et Cosmochimica Acta*, *69*(17), 4253-4265.

Epstein, B. L., S. D'Hondt, J. G. Quinn, J. Zhang, and P. E. Hargraves (1998), An effect of dissolved nutrient concentrations on alkenone-based temperature estimates, *Paleoceanography*, *13*(2), 122-126.

Filippova, A., M. Kienast, M. Frank, and R. R. Schneider (2016), Alkenone paleothermometry in the North Atlantic: A review and synthesis of surface sediment data and calibrations, *Geochemistry, Geophysics, Geosystems*, *17*(4), 1370-1382.

Fischer, G., et al. (2009), Mineral ballast and particle settling rates in the coastal upwelling system off NW Africa and the South Atlantic, *International Journal of Earth Sciences*, *98*(2), 281-298.

Flores, J. A., and F. J. Sierro (2007), Paleoceanography, biological proxies: Coccoliths, in *Encyclopedia of Quaternary Science*, edited by E. A. Scott, pp. 1634-1647, Eselvier, Amsterdam.

Goff, J. A., A. H. Reed, G. Gawarkiewicz, P. S. Wilson, and D. P. Knobles (2019), Stratigraphic analysis of a sediment pond within the New England Mud Patch: New constraints from high-resolution chirp acoustic reflection data, *Marine Geology*, *412*(81-94).

Gong, C., and D. J. Hollander (1997), Differential contribution of bacteria to sedimentary organic matter in oxic and anoxic environments, Santa Monica Basin, California, *Organic Geochemistry*, *26*(9), 545-563.

Gong, C., and D. J. Hollander (1999), Evidence for differential degradation of alkenones under contrasting bottom water oxygen conditions: implication for paleotemperature reconstruction, *Geochimica et Cosmochimica Acta*, *63*(3), 405-411.

Goñi, M. A., D. M. Hartz, R. C. Thunell, and E. Tappa (2001), Oceanographic considerations for the application of the alkenone-based paleotemperature U37K′ index in the Gulf of California, *Geochimica et Cosmochimica Acta*, *65*(4), 545-557.

Grice, K., W. C. M. Klein Breteler, S. Schouten, V. Grossi, J. W. de Leeuw, and J. S. S. Damsté (1998), Effects of zooplankton herbivory on biomarker proxy records, *Paleoceanography*, *13*(6), 686-693.

Grimalt, J. O., J. Rullkötter, M.-A. Sicre, R. Summons, J. Farrington, H. R. Harvey, M. Goñi, and K. Sawada (2000), Modifications of the C37 alkenone and alkenoate composition in the water column and sediment: Possible implications for sea surface temperature estimates in paleoceanography, *Geochemistry, Geophysics, Geosystems*, *1*(11), n/a-n/a.

Hanke, U. M., L. Wacker, N. Haghipour, M. W. I. Schmidt, T. I. Eglinton, and C. P. McIntyre (2017), Comprehensive radiocarbon analysis of benzene polycarboxylic acids (BPCAs) derived from pyrogenic carbon in environmental samples, *Radiocarbon*, *59*(4), 1103-1116.

Hedges, J. I., and R. G. Keil (1995), Sedimentary organic matter preservation: an assessment and speculative synthesis, *Marine Chemistry*, *49*(2), 81-115.

Hoefs, M. J. L., G. J. M. Versteegh, W. I. C. Rijpstra, J. W. de Leeuw, and J. S. S. Damsté (1998), Postdepositional oxic degradation of alkenones: Implications for the measurement of palaeo sea surface temperatures, *Paleoceanography*, *13*(1), 42-49.

Hwang, J., S. J. Manganini, D. B. Montluçon, and T. I. Eglinton (2009), Dynamics of particle export on the Northwest Atlantic margin, *Deep Sea Research Part I: Oceanographic Research Papers*, *56*(10), 1792-1803.

Hwang, J., M. Kim, J. Park, S. J. Manganini, D. B. Montluçon, and T. I. Eglinton (2014), Alkenones as tracers of surface ocean temperature and biological pump processes on the Northwest Atlantic margin, *Deep Sea Research Part I: Oceanographic Research Papers*, *83*, 115-123.

Hwang, J., J. Blusztajn, L. Giosan, M. Kim, S. J. Manganini, D. Montluçon, J. M. Toole, and T. I. Eglinton (2021), Lithogenic Particle Transport Trajectories on the Northwest Atlantic Margin, *Journal of Geophysical Research: Oceans*, *126*(1), e2020JC016802.

Inthorn, M., V. Mohrholz, and M. Zabel (2006a), Nepheloid layer distribution in the Benguela upwelling area offshore Namibia, *Deep Sea Research Part I: Oceanographic Research Papers*, *53*(8), 1423-1438.

Inthorn, M., T. Wagner, G. Scheeder, and M. Zabel (2006b), Lateral transport controls distribution, quality, and burial of organic matter along continental slopes in high-productivity areas, *Geology*, *34*(3), 205-208.

Jaeschke, A., M. Wengler, J. Hefter, T. A. Ronge, W. Geibert, G. Mollenhauer, R. Gersonde, and F. Lamy (2017), A biomarker perspective on dust, productivity, and sea surface temperature in the Pacific sector of the Southern Ocean, *Geochimica et Cosmochimica Acta*, *204*, 120-139.

Keil, R. G., and L. M. Mayer (2014), Mineral matrices and organic matter., in *Treatise on Geochemistry*, edited, pp. 337-359, Elservier.

Keil, R. G., D. B. Montlucon, F. G. Prahl, and J. I. Hedges (1994a), Sorptive preservation of labile organic matter in marine sediments, *Nature*, *370*, 549-552.

Keil, R. G., E. Tsamakis, C. B. Fuh, J. C. Giddings, and J. I. Hedges (1994b), Mineralogical and textural controls on the organic composition of coastal marine sediments: Hydrodynamic separation using SPLITT-fractionation, *Geochimica et Cosmochimica Acta*, *58*(2), 879-893.

Kienast, M., G. MacIntyre, N. Dubois, S. Higginson, C. Normandeau, C. Chazen, and T. D. Herbert (2012), Alkenone unsaturation in surface sediments from the eastern equatorial Pacific: Implications for SST reconstructions, *Paleoceanography*, *27*(1).

Kusch, S., T. I. Eglinton, A. C. Mix, and G. Mollenhauer (2010), Timescales of lateral sediment transport in the Panama Basin as revealed by radiocarbon ages of alkenones, total organic carbon and foraminifera, *Earth and Planetary Science Letters*, *290*(3–4), 340-350.

Laine, E. P., and C. D. Hollister (1981), Geological effects of the Gulf Stream System on the northern Bermuda Rise, *Marine Geology*, *39*(3), 277-310.

Laine, E. P., W. D. Gardner, M. Jo Richardson, and M. Kominz (1994), Abyssal currents and advection of resuspended sediment along the northeastern Bermuda Rise, *Marine Geology*, *119*(1), 159-171.

Locarnini, R. A., et al. (2019), World Ocean Atlas 2018, Volume 1: Temperature. A. Mishonov, Technical Editor., *NOAA Atlas NESDIS*, *81*, 52.

Magill, C. R., B. Ausín, P. Wenk, C. McIntyre, L. Skinner, A. Martínez-García, D. A. Hodell, G. H. Haug, W. Kenney, and T. I. Eglinton (2018), Transient hydrodynamic effects influence organic carbon signatures in marine sediments, *Nature Communications*, *9*(1), 4690.

Mayer, L. M. (1994a), Surface area control of organic carbon accumulation in continental shelf sediments, *Geochimica et Cosmochimica Acta*, *58*(4), 1271-1284.

Mayer, L. M. (1994b), Relationships between mineral surfaces and organic carbon concentrations in soils and sediments, *Chemical Geology*, *114*(3), 347-363.

McCave, I. N., and I. R. Hall (2006a), Size sorting in marine muds: Processes, pitfalls, and prospects for paleoflow-speed proxies, *Geochemistry, Geophysics, Geosystems*, *7*(10), n/a-n/a.

McCave, I. N., and I. R. Hall (2006b), Size sorting in marine muds: Processes, pitfalls, and prospects for paleoflow-speed proxies, *Geochemistry, Geophysics, Geosystems*, *7*(10).

McCave, I. N., B. Manighetti, and S. G. Robinson (1995), Sortable silt and fine sediment size/composition slicing: Parameters for palaeocurrent speed and palaeoceanography, *Paleoceanography*, *10*(3), 593-610.

McIntyre, C. P., L. Wacker, N. Haghipour, T. M. Blattmann, S. Fahrni, M. Usman, T. I. Eglinton, and H.-A. Synal (2016), Online 13C and 14C Gas Measurements by EA-IRMS–AMS at ETH Zürich, *Radiocarbon*, *59*(3), 893-903.

Mollenhauer, G., and T. I. Eglinton (2007), Diagenetic and sedimentological controls on the composition of organic matter preserved in California Borderland Basin sediments, *Limnology and Oceanography*, *52*(2), 558-576.

Mollenhauer, G., T. I. Eglinton, E. C. Hopmans, and J. S. Sinninghe Damsté (2008), A radiocarbon-based assessment of the preservation characteristics of crenarchaeol and alkenones from continental margin sediments, *Organic Geochemistry*, *39*(8), 1039-1045.

Mollenhauer, G., M. Inthorn, T. Vogt, M. Zabel, J. S. Sinninghe Damsté, and T. I. C. Q. Eglinton (2007), Aging of marine organic matter during cross-shelf lateral transport in the Benguela upwelling system revealed by compound-specific radiocarbon dating, *Geochemistry, Geophysics, Geosystems*, *8*, Q09004.

Mollenhauer, G., T. I. Eglinton, N. Ohkouchi, R. R. Schneider, P. J. Müller, P. M. Grootes, and J. Rullkötter (2003), Asynchronous alkenone and foraminifera records from the Benguela Upwelling System, *Geochimica et Cosmochimica Acta*, *67*, 2157-2171.

Mollenhauer, G., M. Kienast, F. Lamy, H. Meggers, R. R. Schneider, J. M. Hayes, and T. I. C. P. A. Eglinton (2005), An evaluation of 14C age relationships between co-occurring foraminifera, alkenones, and total organic carbon in continental margin sediments, *Paleoceanography*(1), PA1016.

Müller, P. J., G. Kirst, G. Ruhland, I. von Storch, and A. Rosell-Melé (1998), Calibration of the alkenone paleotemperature index U37K' based on core-tops from the eastern South Atlantic and the global ocean (60°N-60°S), *Geochimica et Cosmochimica Acta*, *62*, 1757-1772.

Ohkouchi, N., T. I. Eglinton, L. D. Keigwin, and J. M. Hayes (2002), Spatial and Temporal Offsets Between Proxy Records in a Sediment Drift, *Science*, *298*(5596), 1224-1227.

Ohkouchi, N., L. Xu, C. M. Reddy, D. Montluon, and T. I. linton (2005), Radiocarbon dating of alkenones from marine sediments: I. Isolation Protocol *Radiocarbon*, *47*, 401-412.

Pak, H., L. A. Codispoti, and J. R. V. Zaneveld (1980), On the intermediate particle maxima associated with oxygen-poor water off western South America, *Deep Sea Research Part A. Oceanographic Research Papers*, *27*(10), 783-797.

Pedrosa-Pàmies, R., A. Sanchez-Vidal, A. Calafat, M. Canals, and R. Durán (2013), Impact of storm-induced remobilization on grain size distribution and organic carbon content in sediments from the Blanes Canyon area, NW Mediterranean Sea, *Progress in Oceanography*, *118*, 122-136.

Prahl, F. G., and S. G. Wakeham (1987), Calibration of unsaturation patterns in long-chain ketone compositions for palaeotemperature assessment, *Nature*, *330*, 367-369.

Prahl, F. G., L. A. Muehlhausen, and D. L. Zahnle (1988), Further evaluation of long-chain alkenones as indicators of paleoceanographic conditions, *Geochimica et Cosmochimica Acta*, *52*(9), 2303-2310.

Prahl, F. G., J. F. Rontani, N. Zabeti, S. E. Walinsky, and M. A. Sparrow (2010), Systematic pattern in U37K′ – Temperature residuals for surface sediments from high latitude and other oceanographic settings, *Geochimica et Cosmochimica Acta*, *74*(1), 131-143.

Premuzic, E. T., C. M. Benkovitz, J. S. Gaffney, and J. J. Walsh (1982), The nature and distribution of organic matter in the surface sediments of world oceans and seas, *Organic Geochemistry*, *4*(2), 63-77.

Raja, M., and A. Rosell-Melé (2021), Appraisal of sedimentary alkenones for the quantitative reconstruction of phytoplankton biomass, *Proceedings of the National Academy of Sciences*, *118*(2), e2014787118.

Reimers, C. E., and E. Suess (1983), Spatial and temporal patterns of organic matter accumulation on the Peru continental margin, in *Coastal upwelling, its sediment record. Part B: sedimentary records of ancient coastal upwelling*, edited by J. Thiede and E. Suess, pp. 311-345, New York.

Rein, B., A. Lückge, L. Reinhardt, F. Sirocko, A. Wolf, and W.-C. Dullo (2005), El Niño variability off Peru during the last 20,000 years, *Paleoceanography*, *20*(4).

Rontani, J. F., J. K. Volkman, F. G. Prahl, and S. G. Wakeham (2013), Biotic and abiotic degradation of alkenones and implications for U37K′ paleoproxy applications: A review, *Organic Geochemistry*, *59*, 95-113.

Rosell-Melé, A., and F. G. Prahl (2013), Seasonality of UK′37 temperature estimates as inferred from sediment trap data, *Quaternary Science Reviews*, *72*, 128-136.

Rosell-Melé, A., G. Eglinton, U. Pflaumann, and M. Sarnthein (1995), Atlantic core-top calibration of the U37K index as a sea-surface palaeotemperature indicator, *Geochimica et Cosmochimica Acta*, *59*(15), 3099-3107.

Rühlemann, C., and M. Butzin (2006), Alkenone temperature anomalies in the Brazil-Malvinas Confluence area caused by lateral advection of suspended particulate material, *Geochemistry, Geophysics, Geosystems*, *7*(10).

Sachs, J. P., and R. F. Anderson (2003), Fidelity of alkenone paleotemperatures in southern Cape Basin sediment drifts, *Paleoceanography*, *18*(4).

Sachs, J. P., R. R. Schneider, T. I. Eglinton, K. H. Freeman, G. Ganssen, J. F. McManus, and D. W. C. Oppo (2000), Alkenones as paleoceanographic proxies, *Geochemistry, Geophysics, Geosystems*, *1*, 1035.

Schaaf, M., and J. Thurow (1995), Late Pleistocene–Holocene climatic cycles recorded in Santa Barbara Basin sediments: interpretation of color density logs from Site 893, *Proceedings ODP Scientific Results*, *146*, 31-44.

Schlitzer, R. (2021), Ocean Data View, odv.awi.de., edited.

Sikes, E. L., J. W. Farrington, and L. D. Keigwin (1991), Use of the alkenone unsaturation ratio U37k to determine past sea surface temperatures: core-top SST calibrations and methodology considerations, *Earth and Planetary Science Letters*, *104*(1), 36-47.

Synal, H.-A., M. Stocker, and M. Suter (2007), MICADAS: A new compact radiocarbon AMS system, *Nuclear Instruments and Methods in Physics Research Section B: Beam Interactions with Materials and Atoms*, *259*(1), 7-13.

Teece, M. A., J. M. Getliff, J. W. Leftley, R. J. Parkes, and J. R. Maxwell (1998), Microbial degradation of the marine prymnesiophyte Emiliania huxleyi under oxic and anoxic conditions as a model for early diagenesis: long chain alkadienes, alkenones and alkyl alkenoates, *Organic Geochemistry*, *29*(4), 863-880.

Tierney, J. E., and M. P. Tingley (2018), BAYSPLINE: A New Calibration for the Alkenone Paleothermometer, *Paleoceanography and Paleoclimatology*, *33*(3), 281-301.

Twichell, D. C., C. E. McClennen, and B. Butman (1981), Morphology and processes associated with the accumulation of the fine-grained deposit on the sourthern New England shelf., *Journal of Sedimentary Petrology*, *51*, 269-280.

Tyrrell, T., and A. Merico (2004), Emiliania huxleyi: bloom observations and the conditions that induce them, in *Coccolithophores: From Molecular Processes to Global Impact*, edited by H. R. Thierstein and J. R. Young, pp. 75-97, Springer Berlin Heidelberg, Berlin, Heidelberg.

Volkman, J. K., G. Eglinton, E. D. S. Corner, and T. E. V. Forsberg (1980), Long-chain alkenes and alkenones in the marine coccolithophorid *Emiliania huxleyi*, *Phytochemistry*, *19*, 2619–2622.

Wacker, L., M. Christl, and H. A. Synal (2010), Bats: A new tool for AMS data reduction, *Nuclear Instruments and Methods in Physics Research Section B: Beam Interactions with Materials and Atoms*, *268*(7), 976-979.

Wefer, G., P. Heinze, and E. Suess (1990), Stratigraphy and sedimentation rates from oxygen isotope composition, organic carbon content, and grain-size distribution at the Peru upwelling region: Holes 680B and 686B, *Proceedings ODP Scientific Results*, *112*.

Zabeti, N., P. Bonin, J. K. Volkman, I. D. Jameson, S. Guasco, and J.-F. Rontani (2010), Potential alteration of U37K′ paleothermometer due to selective degradation of alkenones by marine bacteria isolated from the haptophyte Emiliania huxleyi, *FEMS Microbiology Ecology*, *73*(1), 83-94.

Zonneveld, K. A. F., et al. (2010), Selective preservation of organic matter in marine environments; processes and impact on the sedimentary record, *Biogeosciences*, *7*(2), 483-511.

645

650

655